



Contents lists available at ScienceDirect

Journal of Colloid and Interface Science

www.elsevier.com/locate/jcis



In situ ATR–FTIR and surface complexation modeling studies on the adsorption of dimethylarsinic acid and *p*-arsanilic acid on iron-(oxyhydr)oxides

William Mitchell^a, Sabine Goldberg^b, Hind A. Al-Abadleh^{a,*}

^a Chemistry Department, Wilfrid Laurier University, Waterloo, Canada ON N2L 3C5

^b USDA-ARS, US Salinity Laboratory, Riverside, CA 92507, USA

ARTICLE INFO

Article history:

Received 17 November 2010

Accepted 15 February 2011

Available online 24 February 2011

Keywords:

Dimethylarsinic acid

p-Arsanilic acid

Iron (oxyhydr)oxides

ATR–FTIR

Triple-layer surface complexation model

ABSTRACT

Arsenic is an element that exists naturally in many rocks and minerals around the world. It also accumulates in petroleum, shale, oil sands, and coal deposits as a result of biogeochemical processes, and it has been found in fly ash from the combustion of solid biofuels. Arsenic compounds in their organic and inorganic forms pose both a health and an environmental risk, and continue to be a challenge to the energy industry. The environmental fate and removal technologies of arsenic compounds are controlled to a large extent by their surface interactions with inorganic and organic adsorbents. We report thermodynamic binding constants, K_{binding} , from applying the triple-layer surface complexation model to adsorption isotherm and pH envelope data for dimethylarsinic acid (DMA) and *p*-arsanilic acid (*p*-AsA) on hematite and goethite. Ligand exchange reactions were constructed based on the interpretation of ATR–FTIR spectra of DMA and *p*-AsA surface complexes. Surface coverage of adsorbates was quantified in situ from the spectral component at 840 cm^{-1} . The best fit to the DMA adsorption data was obtained using outer-sphere complex formation, whereas for *p*-AsA, the best fit was obtained using two monodentate inner-sphere surface complexes. The significance of the results is discussed in relation to improving modeling tools used by environmental regulators and the energy sector for optimum control of arsenic content in fuels.

© 2011 Elsevier Inc. All rights reserved.

1. Introduction

The current state of knowledge on the distribution, speciation, uses, metabolism, fate, remediation, and regulation of arsenic has been published in two excellent recent books [1,2]. Arsenic is an element that exists naturally in many rocks and minerals around the world. It also accumulates in petroleum, shale, oil sands, and coal deposits as a result of biogeochemical processes [3,4], and it has been found in fly ash from the combustion of solid biofuels [5]. Once liberated due to natural weathering or human activities, it takes the form of the inorganic species arsenate, iAs(V) , and arsenite, iAs(III) . The latter species could be methylated by a number of microorganisms depending on the level of microbial activity and soil conditions [2]. The bioproduction of methylated arsenicals, which include monomethylarsonic acid (MMA) and dimethylarsinic acid (DMA), has been explained by the Challenger Pathway [2]. Eventually, arsenic can be lost to the atmosphere through biovolatilization from soils with high arsenic concentrations and lots of microorganisms. Moreover, methylated arsenicals have historically been used as herbicides and pesticides on cotton fields and golf courses, causing elevated arsenic concentrations in surface and groundwater [6]. In Canada, MMA was used to control mountain

pine beetles in British Columbia [7]. The disposal of arsenic-containing waste (mostly electronics) in landfills also contaminates groundwater with arsenic and releases arsine gases to the atmosphere at concentrations above background levels (ca. 0.1–2 ppt) [8–10].

In addition, *organic forms of arsenic*, including methylated and aromatic compounds, are synthesized during the pyrolysis of oil shale [3,11,12]. Arsenic content in energy sources continues to be a challenge to the energy industry because these compounds are potent catalyst poisons, hindering the optimum use of these fuels and their conversion into useful feedstocks [3]. For example, coal-derived syngas (largely CO and H_2) contains arsenic species that deactivate the $\text{Cu/ZnO/Al}_2\text{O}_3$ catalyst used for producing methanol, a promising fuel for internal combustion engines, fuel cells, and a source of hydrogen [13]. Moreover, compounds such as *p*-arsanilic acid (4-aminobenzenearsonic acid, *p*-AsA) and roxarsone (4-hydroxy-3-nitrobenzenearsonic acid, ROX) are used as feed additives in the poultry industry [14,15] and are introduced into the environment through disposal and land application of contaminated poultry litter [14]. The biogeochemical transformation of these compounds to inorganic arsenic occurs a result of enhanced microbial activity and/or exposure to UV radiation [16]. The toxicity of arsenic compounds to humans varies with the chemical form and oxidation state. In general, all the trivalent forms of arsenic, including methylated ones, are genotoxic (capable of

* Corresponding author.

E-mail address: halabadleh@wlu.ca (H.A. Al-Abadleh).

causing genetic disorders) and are more toxic than the corresponding pentavalent forms. Hence, it is clear that arsenic compounds in their organic and inorganic forms continue to be a challenge to the energy industry and pose both a health and an environmental risk [17].

The environmental fate and removal technologies of arsenic compounds are controlled to a large extent by their surface interactions with inorganic and organic adsorbents. These interactions have been studied extensively for arsenate and arsenite on a number of metal oxide and mineral substrates using surface sensitive spectroscopic techniques, and complemented by quantum chemical calculations and surface complexation modeling [18–23]. This excellent body of published work highlighted the need for experiments on the surface chemistry of organoarsenicals. To date, the number of batch studies on the factors that affect the adsorption and desorption of organoarsenicals on Fe-, Al- and Ti-(oxyhydr)oxides [24–33] exceeds that of in situ surface sensitive measurements using techniques such as attenuated total internal reflection spectroscopy (ATR–FTIR) [30,34–36] and X-ray absorption spectroscopy (XAS) [27,30]. Surface complexation models (SCMs) have been used to describe the adsorption of methylated arsenic species on hydrous iron oxide [25] and nanocrystalline titanium oxide [27]. The triple-layer model was applied to describe DMA adsorption on hydrous ferric oxide using a monodentate inner-sphere surface complex. To obtain a good fit, it was necessary to assume two sets of reactive surface sites having differing adsorption affinities [25]. The charge distribution multisite complexation (MUSIC) model was applied to describe DMA adsorption on titanium oxide using an inner-sphere surface complex observed with XAS [27]. However, the As–Ti distance observed with XAS could also be explained by the formation of hydrogen bonds between the oxygen atom on DMA and a protonated hydroxyl group on the titanium oxide surface. Adsorption of DMA onto goethite was found to be independent of solution ionic strength, indicative of an inner-sphere adsorption mechanism [33]. At the same time, adsorption of DMA did not shift the point of zero charge, indicative of an outer-sphere adsorption mechanism [33]. The triple-layer model has not yet been applied to describe DMA adsorption on goethite. It was concluded that DMA adsorbed as a monodentate complex on goethite because it replaced only phosphate adsorbed as a monodentate species [32].

In this work, we report detailed triple-layer SCM results on experimental data collected for DMA and p-AsA adsorption on hematite and goethite using ATR–FTIR. Relative to arsenate, these two organoarsenicals replace hydroxyl groups with two methyl and one aromatic groups, respectively. We examined earlier the effect of organic substitution and protonation on the stretching frequency of As–O groups, $\nu(\text{As–O})$ [37,38]. Here, spectroscopic investigations of the adsorption isotherms of DMA on hematite and goethite were carried out – for the first time using ATR–FTIR – using solution concentrations as low as 1 μM at pH 7 and $I = 0.01$ M. The adsorption isotherms of p-AsA from ATR–FTIR measurements were reported earlier [35] at pH 7, where values of binding constants were extracted from Langmuir model fits. Derivation of the triple layer reported herein is based on the nature of surface complexes reported by our group for DMA [38] and p-AsA [36] as a function of pH using ATR–FTIR. Adsorption isotherms and pH envelopes generated from spectral data highlight the usefulness of ATR–FTIR as a technique in constructing in situ correlations between surface coverage quantified from spectral components and aqueous phase concentrations and solution pH, respectively. This is in contrast to isotherms and pH envelopes generated from the “total arsenic content” analysis in ex situ bulk batch studies. As discussed in detail below, using ATR–FTIR for quantitative measurements of in situ surface coverage is limited by the ability to measure – directly or indirectly – certain constants for the

adsorbent and adsorbate. The significance of our studies is discussed in terms of improving modeling tools used by environmental regulators, and the usefulness of iron-based materials in developing arsenical removal technologies.

2. Experimental and modeling procedures

2.1. Chemical

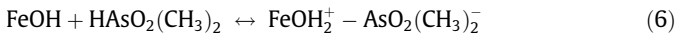
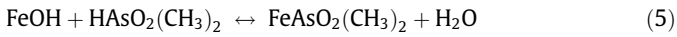
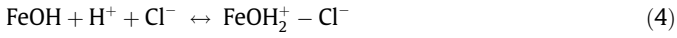
Stock solutions of DMA (cacodylic acid sodium salt trihydrate, $\text{C}_2\text{H}_6\text{AsO}_2\text{Na}\cdot 3\text{H}_2\text{O}$, Alfa Aesar, used as received) were prepared by dissolving the powder in concentrated NaOH (EMD, ACS grade) with continuous mechanical stirring, and then lowering the pH using HCl (Ricca Chemical, 6 N). *Caution: DMA is highly toxic via inhalation and skin contact and is a carcinogen.* Ionic strength was adjusted using KCl (99.5%, EM Science). A series of DMA concentrations were prepared from the stock solutions in the range from 0.001 to 100 mM using Millipore water (18.2 M Ω). The Fe-(oxyhydr)oxides used herein are hematite ($\alpha\text{-Fe}_2\text{O}_3$, >99.9%, Nanostructured and Amorphous Materials), and goethite ($\alpha\text{-FeOOH}$, >99.9%, Alfa Aesar). Determination of BET surface area, particle size, and isoelectric points (IEP) was reported earlier [35]: 19 m²/g, 67 nm average diameter, and 8.6 for spherical $\alpha\text{-Fe}_2\text{O}_3$ particles, and 21 m²/g, 0.1–0.9 μm (average length along *a* axis), and 8.8 for needle-shaped $\alpha\text{-FeOOH}$ particles, respectively. Details on the experimental procedure for preparing thin Fe-(oxyhydr)oxide films on the ATR internal reflection element (IRE) were described in the Supporting Information (SI) of reference [35]. Briefly, $\alpha\text{-Fe}_2\text{O}_3$ films were prepared by making a slurry 14 mg sample in an 1.5 mL water/ethanol mixture (1:0.4 (v/v)). Slurries of $\alpha\text{-FeOOH}$ particles were prepared by mixing 16 mg sample of ground goethite (Wig-L-Bug, 1 min) in a 0.75 mL ethanol. Each slurry was then ultrasonicated for 1 h and then spread over a clean and dry ZnSe ATR crystal and allowed to dry overnight in air at room temperature. A freshly deposited film was prepared for each adsorption isotherm experiment.

2.2. ATR–FTIR experiments

ATR–FTIR spectra were collected using a HATRPlus accessory (Pike Technologies) installed in a Nicolet 8700 FTIR spectrometer (Thermo Instruments) equipped with a MCT detector. The 100 μL ATR flow cell houses a 60° ZnSe crystal as the IRE (80 \times 10 \times 4 mm) on which the Fe-(oxyhydr)oxide films were directly deposited. To introduce the liquid phase, the ATR flow cell was connected to a compact pump (Masterflex L/S) using Tygon tubes (0.8 mm I.D., Masterflex). The detection limit of the ATR flow cell to DMA(aq) was determined to be 8 mM. All spectra were collected at 4 cm^{-1} resolution by averaging 300 scans. Prior to each adsorption experiment, an ATR–FTIR single beam spectrum of dry Fe-(oxyhydr)oxide films was collected and then a background solution ($I = 0.01$ M and pH 7) was flowed across for at least 60 min at a rate of 1 mL/min before a spectrum is collected. Each DMA solution was flowed across the wetted film for 15 min at rate of 1 mL/min starting from the low concentration. Absorbance spectra were generated by referencing single-beam spectra collected for DMA(aq) in equilibrium with the film to the background solution in contact with the film. DMA solutions with concentrations higher than the detection limit were collected from the exit port of the ATR flow cell. ATR–FTIR spectra of these solutions were collected on clean dry ZnSe crystal (no film) after each adsorption experiment. Absorbance spectra of DMA(aq) with concentrations >8 mM were subtracted from the those obtained from DMA(aq) in equilibrium with the film. This data treatment ensured the elimination of spectral components originating from unbound DMA species.

2.3. Surface complexation modeling

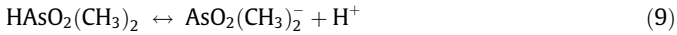
The triple-layer model [39,40] was used to describe the adsorption of DMA and p-AsA onto hematite and goethite. In the present application of the model, the following surface complexation constants were considered,



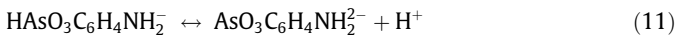
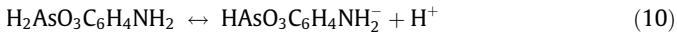
or



where FeOH represents reactive surface hydroxyl groups on hematite and goethite. Even though the surface complexation reactions are written starting with the completely undissociated acids, the model application contains the aqueous speciation reaction(s) for DMA and pAsA:



or



Equilibrium constant expressions for the surface complexation constants are

$$K_+(\text{int}) = \frac{[\text{FeOH}_2^+]}{[\text{FeOH}][\text{H}^+]} \exp(F\psi_o/RT) \quad (12)$$

$$K_-(\text{int}) = \frac{[\text{FeO}^-][\text{H}^+]}{[\text{FeOH}]} \exp(-F\psi_o/RT) \quad (13)$$

$$K_{\text{K}^+}(\text{int}) = \frac{[\text{FeO}^- - \text{K}^+][\text{H}^+]}{[\text{FeOH}][\text{K}^+]} \exp[F(\psi_\beta - \psi_o)/RT] \quad (14)$$

$$K_{\text{Cl}^-}(\text{int}) = \frac{[\text{FeOH}_2^+ - \text{Cl}^-]}{[\text{FeOH}][\text{H}^+][\text{Cl}^-]} \exp[F(\psi_o - \psi_\beta)/RT] \quad (15)$$

$$K_{\text{DMA}}^{\text{is}}(\text{int}) = \frac{[\text{FeAsO}_2(\text{CH}_3)_2]}{[\text{FeOH}][\text{HAsO}_2(\text{CH}_3)_2]} \quad (16)$$

$$K_{\text{DMA}}^{\text{os}}(\text{int}) = \frac{[\text{FeOH}_2^+ - \text{AsO}_2(\text{CH}_3)_2^-]}{[\text{FeOH}][\text{HAsO}_2(\text{CH}_3)_2]} \exp[F(\psi_o - \psi_\beta)/RT] \quad (17)$$

or

$$K_{\text{p-AsA}}^{\text{is}}(\text{int}) = \frac{[\text{FeHASO}_3\text{C}_6\text{H}_4\text{NH}_2]}{[\text{FeOH}][\text{H}_2\text{AsO}_3\text{C}_6\text{H}_4\text{NH}_2]} \quad (18)$$

$$K_{\text{p-AsA}}^{\text{os}}(\text{int}) = \frac{[\text{FeAsO}_3\text{C}_6\text{H}_4\text{NH}_2^-][\text{H}^+]}{[\text{FeOH}][\text{H}_2\text{AsO}_3\text{C}_6\text{H}_4\text{NH}_2]} \exp(-F\psi_o/RT), \quad (19)$$

where F is the Faraday constant (C mol^{-1}), ψ is the surface potential (V), R is the molar gas constant ($\text{J mol}^{-1} \text{K}^{-1}$), T is the absolute tem-

perature (K), and square brackets indicate concentrations (mol L^{-1}). The exponential terms can be considered as solid phase activity coefficients.

The computer program FITELQ (3.2) [41] was used to fit the DMA and p-AsA surface complexation constants to the experimental adsorption data. The FITELQ code uses a nonlinear least-squares optimization routine to fit equilibrium constants to experimental data and contains the triple-layer model. To describe adsorption we used either an inner-sphere or an outer-sphere monodentate surface species for DMA and two inner-sphere monodentate surface species for p-AsA. The model failed to converge when both an inner-sphere and an outer-sphere surface complex were included. Parameter values were fixed at $\log K_+(\text{int}) = 4.3$, $\log K_-(\text{int}) = -9.8$, $\log K_{\text{K}^+}(\text{int}) = -9.3$, $\log K_{\text{Cl}^-}(\text{int}) = 5.4$, $C_1 = 1.2 \text{ F m}^{-2}$, $C_2 = 0.2 \text{ F m}^{-2}$, considered optimal for goethite by Zhang and Sparks [42]. We used parameter values for goethite for both Fe-(oxyhydr)oxides, since values for hematite were not available.

3. Results

3.1. ATR-FTIR spectra of DMA(ads) on Fe-(oxyhydr)oxides at pH 7

Fig. 1 shows the ATR-FTIR spectra of adsorbed DMA, DMA(ads), on (a) $\alpha\text{-Fe}_2\text{O}_3$ and (b) $\alpha\text{-FeOOH}$ films at pH 7 and $I = 0.01 \text{ M KCl}$ and as a function of DMA(aq) concentrations (5–800 μM). These absorbance spectra were collected in situ after 15 min equilibrium with a given concentration of DMA(aq) by referencing to the clean films in equilibrium with the 0.01 M electrolyte solution. At pH 7, the deprotonated form of DMA is the most dominant species in the aqueous phase. Surface sites at this pH are a mix of neutral ($\equiv\text{FeOH}$) and positively charged ($\equiv\text{FeOH}_2^+$), with a higher

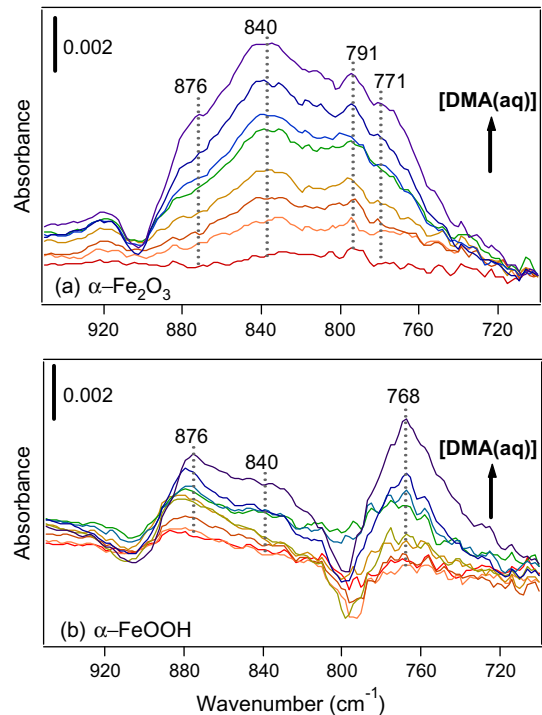


Fig. 1. Representative ATR-FTIR absorbance spectra of DMA(ads) on (a) $\alpha\text{-Fe}_2\text{O}_3$ and (b) $\alpha\text{-FeOOH}$ as a function of DMA concentration (from bottom): (a) 0.005, 0.01, 0.03, 0.05, 0.1, 0.15, 0.25, 0.5, and 0.8 mM, and (b) 0.005, 0.01, 0.03, 0.05, 0.1, 0.15, 0.25, 0.5, and 0.8 mM at pH 7 and $I = 0.01 \text{ M}$. These concentrations are below the detection limit of DMA(aq).

concentration of the latter given that the isoelectric point of the hematite and goethite used in our experiments is around 9. Hence, ligand exchange between surface sites and incoming DMA molecules is driven by favorable electrostatic interactions. The assignment of the spectral components observed in Fig. 1 has been discussed in detail in our recent publication reporting adsorption mechanism of DMA [34].

Briefly, the assignment of the observed frequencies was based on comparison with the spectra of bulk DMA in the liquid ($pK_a = 6.1$) and solid acid and salt phases [37], desorption kinetics due to chloride and phosphate anions, and aided by frequency calculations on geometry-optimized clusters of DMA–iron oxide clusters. Our data suggest the simultaneous formation of inner- and outer-sphere DMA(ads), which gives rise to spectral components in the range 700–880 cm^{-1} . Low frequency components at 771 and 768 cm^{-1} have major contributions from inner-sphere complexes, and hence are assigned to $\nu(\text{As}-\text{OFe})$. The component at 791 cm^{-1} observed in Fig. 1a is assigned to $\nu(\text{As}-\text{O}\cdots\text{H})$ from uncomplexed As–O bonds involved in strong H-bonding as observed for DMA in the solid phases [37]. Additionally, components around 840 cm^{-1} are assigned to $\nu(\text{As}=\text{O})$ from free As=O groups, with bond order of ca. 1.5. Moreover, the component at 876 cm^{-1} is assigned to $\nu(\text{As}=\text{O})$ in outer-sphere complexes as a result of the involvement of the second As–O group in DMA in strong H-bonding that decreases electronic delocalization. The loss feature around 800 cm^{-1} observed in Fig. 1b when compared to Fig. 1a is most likely due to a decrease in the concentration of $\equiv\text{FeOH}$ or $\equiv\text{FeOH}_2^+$ sites [43–45] on FeOOH films as a result of DMA adsorption through H-bonding or ligand exchange mechanisms. In the following sections, we illustrate the usefulness of in situ ATR–FTIR measurements in quantifying the surface coverage of DMA(ads).

3.2. Calculations of DMA surface coverage on porous Fe-(oxyhydr)oxide films from ATR–FTIR

Sperline et al. [46] proposed the following simple model for the quantification of surface coverage, S (molecules/ cm^2), of adsorbates on porous metal oxide films using ATR–FTIR spectroscopy,

$$A(\lambda) = S\varepsilon(\lambda)d_e(\lambda)/d_p(\lambda) + \varepsilon(\lambda)cd_e(\lambda) \quad (20)$$

where $A(\lambda)$ is the baseline-corrected absorbance, $\varepsilon(\lambda)$ is the molar extinction coefficient of the adsorbate in $\text{cm}^2/\text{molecule}$, d_e is the effective pathlength of the IR light in the ATR IRE in cm, d_p is the depth of penetration per reflection in cm, which approximately equals d_e/N , where N is the total number of reflections inside the IRE, and c is the aqueous phase concentration of the molecule of interest. Values of d_e are calculated using the equation:

$$d_e(\lambda) \approx N \cdot d_p(\lambda) = (l/t) \cot \theta \cdot \lambda / [2\pi n_1 \sqrt{\sin^2 \theta - (n_2/n_1)^2}], \quad \text{where } l$$

and t are the length and thickness of the IRE, respectively, θ is the angle of incidence, and n_1 and n_2 are the indices of refraction of the IRE and the sample, respectively. The first term in Eq. (20) treats the adsorbed species as a thin flat layer, and the second term accounts for the contribution of aqueous phase species to the total absorbance at a given wavelength, λ . This model could be used to convert the ATR absorbance at a given λ , provided that $\varepsilon(\lambda)$, d_p , and d_e are estimated accurately for a given molecule [46,47]. It also assumes that $\varepsilon(\lambda)$ for a given vibration in the molecule of interest is the same in the aqueous phase and as an adsorbate.

For our adsorption isotherm experiments reported herein, the second term in Eq. (20) has negligible contribution to the ATR absorbance spectra shown in Fig. 1. This is because concentrations of DMA(aq) in contact with the Fe-(oxyhydr)oxide films are below the detection limit of our IRE to DMA(aq) (8 mM). To take into account the surface area of the Fe-(oxyhydr)oxides porous films

available for adsorption and probed by the IR light, we reported earlier a modified version of Eq. (20) [35],

$$S \text{ (molecules cm}^{-2}\text{)} = \frac{A(\lambda)}{\varepsilon(\lambda)N^2d_p(\lambda)\rho_{\text{bulk}} \cdot S \cdot A_{\text{BET}}}, \quad (21)$$

where ρ_{bulk} is the bulk density of the deposited Fe-(oxyhydr)oxides films estimated from the deposited mass (m), area of IRE covered ($a = 5.0 \text{ cm}^2$) and measured thickness of the films (h): $\rho_{\text{bulk}} = m(\text{g})/[a(\text{cm}^2)h(\text{cm})]$. In the presence of a porous film of hematite and goethite particles on the IRE, the value of n_2 to account for the porosity and the presence of solvent in the pores [48]. A volume-weighted average of the refractive index of the particles (n'_2) is calculated using $n'_2 = F_{\nu} \cdot n_{\text{par}} + (1 - F_{\nu}) \cdot n_{\text{H}_2\text{O}(l)}$ where $F_{\nu} = \rho_{\text{bulk}}(\text{g cm}^{-3})/\rho_{\text{true}}(\text{g cm}^{-3})$. Table S1 in the SI of reference [35] lists values of m , h , and ρ_{true} resulting in $d_p^{840\text{cm}^{-1}} = 2.3 \times 10^{-4}$ and 1.3×10^{-4} cm for $\alpha\text{-Fe}_2\text{O}_3$ - and $\alpha\text{-FeOOH}$ -coated IRE, respectively.

The spectral component at 840 cm^{-1} in Fig. 1 assigned to DMA(ads) was chosen because of its proximity to the most intense component observed at 831 cm^{-1} in the ATR–FTIR spectrum of DMA(aq) at $\text{pH} > 6.1$, which is assigned to $\nu(\text{As}=\text{O})$ in fully deprotonated species. Hence, the value for $\varepsilon(\lambda)$ for DMA(ads) was obtained from the Beer's law fit to a calibration curve constructed for DMA(aq) at $\text{pH} 7$ [$\varepsilon(0.0012 \text{ cm}) = 6 \times 10^{-19} \text{ cm}^2 \text{ molecule}^{-1}$]. Fig. 2a and b shows the adsorption isotherms of DMA on $\alpha\text{-Fe}_2\text{O}_3$ and FeOOH, respectively, at $\text{pH} 7$ and $I = 0.01 \text{ M}$. The left axis displays the absorbance at 840 cm^{-1} , which was converted to S_{DMA} in units of molecule cm^{-2} (right axis) using Eq. (21), and molar ratios units of mmol As/mol Fe (second right axis). Similarly, experimental adsorption isotherm data [35] shown in Fig. 3a and b for p-AsA are expressed in molecule cm^{-2} and molar ratios units using constants reported earlier [35]. The validity of this approach to quantifying S_{DMA} and $S_{\text{p-AsA}}$ from spectral data was verified by bulk measurements of surface coverage from analysis of total arsenic using inductively coupled plasma atomic emission spectroscopy (ICP–AES) [34,35]. The quantification approach reported herein has the advantage of being an in situ cost-effective method (no chemical digestion is needed to release bonded arsenic).

As described in the following section, experimental data shown in Figs. 2 and 3 were modeled using a triple-layer model based on the binding mechanism and the nature of surface complexes elucidated from ATR–FTIR spectroscopy. The model failed to converge when both an inner-sphere and an outer-sphere surface complex were included.

3.3. Surface complexation modeling

The triple-layer model was fit to the DMA adsorption isotherm and pH envelope data on hematite and goethite both as one combined data set and individually. Not surprisingly, the fit for the combined data set (data not shown) was of lower quality than for isotherms and envelopes fit individually. The triple-layer model was able to describe DMA adsorption using either a monodentate inner-sphere surface complex or a monodentate outer-sphere surface complex but not both. The quality of fit, as measured by the overall variance, $V_Y = \text{SOS}/\text{DF}$, where SOS is the weighted sum of squares of the residuals and DF is the degrees of freedom, was improved for the outer-sphere surface complex. Therefore, the results presented in Fig. 2a and c for hematite, and Fig. 2b and d for goethite are for the outer-sphere surface complex. Despite the fact that the spectroscopic results suggested both an inner-sphere and an outer-sphere surface complex, adding the second type of surface species after the first type had been optimized resulted in lack of model convergence. This is a common limitation of the mathematical fitting procedure.

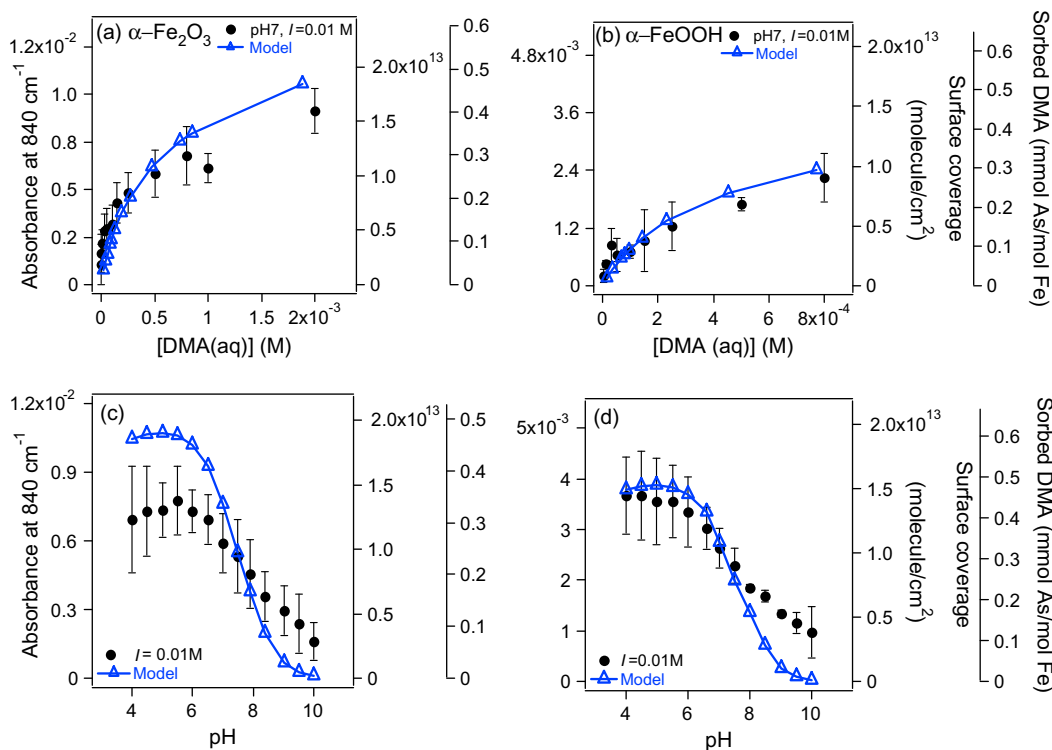


Fig. 2. Adsorption isotherms of DMA on α -Fe₂O₃ and α -FeOOH at 298 K as a function of concentration at pH 7 and $I = 0.01$ M (upper panel), and as a function of pH using 1 mM DMA(aq) ($I = 0.01$ M) (lower panel, with permission from Ref. [34]). Filled circles represent experimental data. Empty triangles represent the fit of the triple-layer model reported here for the first time. Error bars are $\pm\sigma$ from averaging 3–4 experiments, each on a freshly-prepared film.

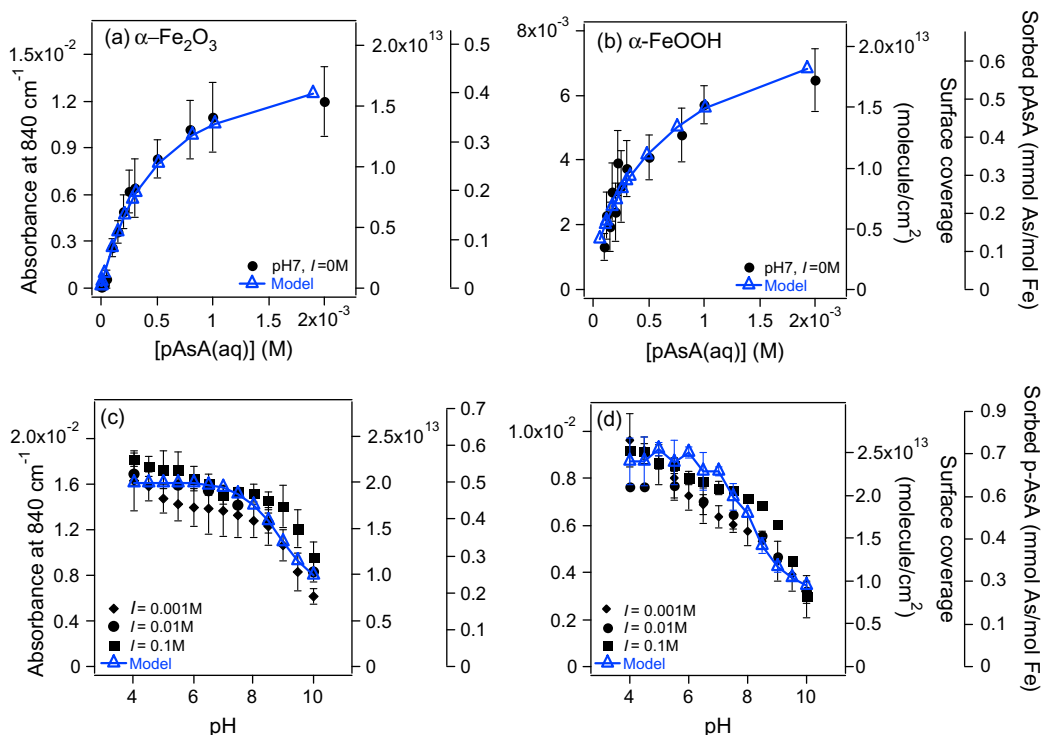


Fig. 3. Adsorption isotherms of p-AsA on α -Fe₂O₃ and α -FeOOH at 298 K as a function of concentration at pH 7 and $I = 0.01$ M (upper panel), and as a function of pH and I using 1 mM p-AsA(aq) (lower panel). Filled circles represent experimental data (with permission from Refs. [35,36]). Empty triangles represent the fit of the triple-layer model reported here for the first time. Error bars are $\pm\sigma$ from averaging 3–4 experiments, each on a freshly-prepared film.

For the adsorption isotherms, the experimental data and model fits for both oxides were not statistically significantly different

from each other (see Fig. 2a and b). For the adsorption envelopes, the experimental data and the model fits were not statistically

Table 1

Triple-layer surface complexation constants for the model fits of DMA and p-AsA adsorption on hematite and goethite at 298 K.

Oxide	$\log K_{\text{DMA}}^{\text{os}}$	SOS/DF	$\log K_{\text{pAsA}}^{\text{is}}$	$\log K_{\text{pAsA}}^{\text{is-}}$	SOS/DF
Hematite					
Combined data	4.30	674	6.49	2.30	345
Isotherm data	4.23	125	5.84	-0.038	36.9
Envelope data	4.53	1138	8.31	1.30	101
Goethite					
Combined data	5.02	720	5.95	1.62	255
Isotherm data	4.33	55.9	6.22	-3.99	24.6
Envelope data	5.63	586	7.32	1.06	124

Notes: Abbreviations stand for: is = inner-sphere, os = outer-sphere, SOS/DF = weighted sum of squares of the residuals, DF = degrees of freedom.

significantly different from each other only in the pH range 4–7.5 for goethite and pH 7–8 for hematite. Thus, for hematite, the model provided only a poor representation of the experimental data.

The triple-layer model was fit to the p-AsA adsorption isotherm and envelope data at three different ionic strengths on hematite and goethite, both as one combined data set and individually. Again, the fits for the combined data sets (data not shown) were of lower quality than for isotherms and envelopes fit individually. The triple-layer model was able to describe p-AsA adsorption using two monodentate inner-sphere surface complexes (see Fig. 3a and c for hematite and Fig. 3b and d for goethite). This adsorption mechanism is in agreement with the spectroscopic results regarding the interpretation of the component at 840 cm^{-1} [36]. For the adsorption isotherms the experimental data and model fits for both oxides were not statistically significantly different from each other (see Fig. 3a and b). For the adsorption envelopes, three ionic strengths were optimized simultaneously. The experimental data and the model fits were not statistically significantly different from each other for $I = 0.01\text{ M}$ in the pH range 4–10 for hematite and pH 4–8 for goethite. Underprediction was observed for $I = 0.1\text{ M}$ above pH 8 and overprediction was found for $I = 0.001\text{ M}$ in the pH range 6–7.5 for hematite and pH 5.5–8 for goethite. This occurred because the model fit showed much less ionic strength dependence than was observed for the experimental adsorption data, especially at $I = 0.001\text{ M}$ (see Fig. 3c and d).

The triple-layer model was able to describe DMA adsorption on both oxides by optimizing just one adjustable parameter, $\log K_{\text{DMA}}^{\text{os}}$, and p-AsA adsorption on both oxides by optimizing two adjustable parameters, $\log K_{\text{pAsA}}^{\text{is}}$ and $\log K_{\text{pAsA}}^{\text{is-}}$ (see Table 1). The quality of the fit was quantitative for the adsorption isotherms of both adsorbates on both adsorbents and at least semi quantitative for the adsorption envelopes. Therefore, the model clearly constitutes an advancement over Langmuir and Freundlich adsorption isotherm approaches, which contain two empirical adjustable parameters and cannot describe changes in adsorption occurring with changes in solution pH.

4. Conclusions and significance

We report thermodynamic binding constants, K_{binding} , from applying the triple-layer SCM to adsorption isotherm and pH envelope data of DMA and p-AsA on hematite and goethite. Ligand exchange reactions were constructed based on the interpretation of ATR-FTIR spectra of DMA and p-AsA surface complexes, particularly the component at 840 cm^{-1} . The best fit to the DMA adsorption data was obtained using outer-sphere complex formation, Eq. (6), whereas for p-AsA, the best fit was obtained using two monodentate inner-sphere surface complexes, Eqs. (7) and (8). We also illustrated the usefulness of ATR-FTIR in calculating in situ surface

coverage of adsorbate from a given spectral component. The significance of these results is provided below.

Extracting values of K_{binding} from experimental adsorption data recorded at equilibrium through mathematical modeling provides insight into the relative affinity of a given chemical to a solid substrate. Despite being a surface phenomenon that is affected by the nature of surface sites, their density and solution pH, values of K_{binding} are often obtained from applying the Langmuir model to experimental data derived from bulk measurements at a given pH and ionic strength [28,30]. Results reported in Table 1 are from the triple-layer SCM applied to experimental data from surface sensitive measurements of surface coverage, and take into account surface charge, solution pH, and the nature of the surface complex elucidated from IR data. Hence, relative affinities (i.e., K_{binding}) of a given organoarsenical to a certain substrate derived from the Langmuir model cannot be compared directly to those derived from SCM. For comparison, the triple-layer SCM used herein was used to fit the DMA adsorption data (isotherm and pH envelope) on goethite at pH 7 of Lafferty and Loeppert [28]. A surface area of $70\text{ m}^2/\text{g}$ was used for goethite in the model [49,50]. We obtained values of surface complexation constants, $\log K_{\text{DMA}}^{\text{os}} = 5.51, 4.77, \text{ and } 5.43$ for combined isotherm and pH envelope, isotherm only, and pH envelope only data, respectively. These constants agree very well with those reported from our spectroscopic studies in Table 1. Moreover, the triple-layer model was previously applied to inorganic arsenate adsorption on amorphous iron oxide by Goldberg and Johnston [51]. Their surface complexation constant, $\log K_{\text{ias}}(\text{V})^{\text{is}} = 5.36$, compares favorably with the data reported in Table 1. Therefore, the triple-layer SCM model derived herein could be used as a more accurate modeling tool by environmental regulators and the energy sector in predicting the uptake of organoarsenicals by iron-rich soils, cleanup adsorbents, and solid catalysts, taking into account properties of the liquid and solid phases.

Acknowledgments

The authors acknowledge funding from Wilfrid Laurier University, WLU Science and Technology Endowment Program (STEP), and the Canadian Foundation for Innovation. Acknowledgment is made to the donors of the American Chemical Society Petroleum Research Fund for support (or partial support) of this research.

References

- [1] R. Ravenscroft, H. Brammer, K. Richards, Arsenic Pollution: A Global Synthesis, Wiley-Blackwell, Malden, MA, 2009.
- [2] W.R. Cullen, Is Arsenic an Aphrodisiac? The Sociochemistry of an Element, RSC Publishing, Cambridge, 2008.
- [3] S.P. Cramer, M. Siskin, L.D. Brown, G.N. George, Energy Fuels 2 (1988) 175.
- [4] F. Li, L.-S. Fan, Energy Environ. Sci. 1 (2008) 248.
- [5] G. Baerthaler, M. Zischka, C. Haraldsson, I. Obernherger, Biomass Bioenergy 30 (2006) 983.
- [6] J. Pelley, Environ. Sci. Technol. A – Pages 39 (2005) 122A.
- [7] K.J. Reimer, W.R. Cullen, Arsenic concentrations in wood, soil and plant tissue collected around trees treated with monosodium methanearsonate (MSMA) for bark beetle control, a report for the BC Ministry of Forests and Range, 2009.
- [8] M. Ponthieu, P. Pinel-Raffaitin, I. Le Hecho, L. Mazeas, D. Amouroux, O. Donard, M. Pontin-Gautier, Water Res. 41 (2007) 3177.
- [9] J.-H. Huang, G. Ilgen, D. Vogel, B. Michalzik, S. Hantsch, L. Tennhardt, B. Bilitewski, Environ. Sci. Technol. 43 (2009) 7092.
- [10] P. Pinel-Raffaitin, I.L. Hecho, D. Amouroux, M. Potin-Gautier, Environ. Sci. Technol. 41 (2007) 4536.
- [11] R.H. Fish, W. Walker, R.S. Tannous, Energy Fuels 1 (1987) 243.
- [12] R.H. Fish, F.E. Brinckman, K.L. Jewett, Environ. Sci. Technol. 16 (1982) 174.
- [13] R. Quinn, T. Mebrahtu, T.A. Dahl, F.A. Lucrezi, B.A. Toseland, Appl. Catal. A 264 (2004) 103.
- [14] Y. Arai, A. Lanzirrotti, S. Sutton, J.A. Davis, D.L. Sparks, Environ. Sci. Technol. 37 (2003) 4083.
- [15] E. Dopp, L.M. Hartmann, A.-M. Florea, A.W. Rettenmeier, A.V. Hirner, Crit. Rev. Toxicol. 34 (2004) 301.
- [16] I. Cortinas, J.A. Filed, M. Kopplin, J.R. Garbarino, A.J. Gandolfi, R. Sierra-Alvarez, Environ. Sci. Technol. 40 (2006) 2951.

- [17] R. Datta, D. Sarkar, S. Sharma, K. Sand, *Sci. Total Environ.* 372 (2006) 39.
- [18] P.A. O'Day, et al. (Eds.), *Advances in Arsenic Research: Integration of Experimental and Observational Studies and Implications for Mitigation*, ACS Symposium Series, Washington, DC, 2005.
- [19] D.L. Sparks, *Metal and oxyanion sorption on naturally occurring oxide and clay mineral surfaces*, in: V.H. Grassian (Ed.), *Environmental Catalysis*, Taylor & Francis Group, Boca Raton, 2005, pp. 3.
- [20] R.T. Cygan, *Molecular modeling in mineralogy and geochemistry*, in: *Reviews in Mineralogy and Geochemistry*, vol. 42, Mineralogical Society of America, Washington, DC, 2001, pp. 1.
- [21] K. Fukushi, D.A. Sverjensky, *Geochem. Cosmochim. Acta* 71 (2007) 3717.
- [22] S. Goldberg, S. Hyun, L.S. Lee, *Vadose Zone J.* 7 (2008) 1231.
- [23] J.G. Hering, S. Dixit, *Contrasting sorption behavior of arsenic(III) and arsenic(V) in suspensions of iron and aluminum oxyhydroxides*, in: P.A. O'Day, et al. (Eds.), *Advances in Arsenic Research: Integration of Experimental and Observational Studies and Implications for Mitigation*, vol. 915, ACS Symposium Series, Washington, DC, 2005, pp. 8.
- [24] Z. Cheng, A.V. Geen, R. Louis, *Environ. Sci. Technol.* 39 (2005) 7662.
- [25] C.D. Cox, M.M. Ghosh, *Water Res.* 28 (1994) 1181.
- [26] B.P. Jackson, W.P. Miller, *Soil Sci. Soc. Am. J.* 64 (2000) 1616.
- [27] C. Jing, M. Xiaogunag, S. Liu, S. Baidas, R. Patraju, C. Christodoulatos, G.P. Korfiatis, *J. Colloid Interface Sci.* 290 (2005) 14.
- [28] B.J. Lafferty, R.H. Loeppert, *Environ. Sci. Technol.* 39 (2005) 2120.
- [29] A. Ramesh, H. Hasegawa, T. Maki, K. Ueda, *Sep. Sci. Technol.* 56 (2007) 90.
- [30] M. Shimizu, M. Ginder-Vogel, S.J. Parikh, D.L. Sparks, *Environ. Sci. Technol.* 44 (2010) 612.
- [31] Zhonghou, C. Jing, F. Li, X. Meng, *Environ. Sci. Technol.* 42 (2008) 2349.
- [32] J.S. Zhang, R.S. Stanforth, S.O. Pehkonen, *J. Colloid Interface Sci.* 317 (2008) 35.
- [33] J.S. Zhang, R.S. Stanforth, S.O. Pehkonen, *J. Colloid Interface Sci.* 306 (2007) 16.
- [34] A. Adamescu, W. Mitchell, I.P. Hamilton, H.A. Al-Abadleh, *Environ. Sci. Technol.* 44 (2010) 7802.
- [35] S. Depalma, S. Cowen, T.N. Hoang, H.A. Al-Abadleh, *Environ. Sci. Technol.* 42 (2008) 1922.
- [36] M. Chabot, T.N. Hoang, H.A. Al-Abadleh, *Environ. Sci. Technol.* 43 (2009) 3142–3147.
- [37] S. Cowen, M. Duggal, T.N. Hoang, H.A. Al-Abadleh, *Can. J. Chem.* 86 (2008) 942.
- [38] A. Adamescu, H. Gray, K. Stewart, I.P. Hamilton, H.A. Al-Abadleh, *Can. J. Chem.* 88 (2010) 65.
- [39] J.A. Davis, R.O. James, J.O. Leckie, *J. Colloid Interface Sci.* 63 (1978) 480.
- [40] K.F. Hayes, J.O. Leckie, *J. Colloid Interface Sci.* 115 (1987) 564.
- [41] A.L. Herbelin, J.C. Westall, FITEQL: a computer program for determination of chemical equilibrium constants from experimental data. Rep. 96, 1996.
- [42] P. Zhang, D.L. Sparks, *Environ. Sci. Technol.* 24 (1990) 1848.
- [43] B. Weckler, H.D. Lutz, *Eur. J. Solid State Inorg. Chem.* 35 (1998) 531.
- [44] D.G. Lumsdon, A.R. Fraser, J.D. Russell, N.T. Livesey, *J. Soil Sci.* 35 (1984) 381.
- [45] S.I. Ikawa, S. Maeda, *Spectrochim. Acta* 24A (1968) 655.
- [46] R.P. Sperline, S. Muralidharan, H. Freiser, *Langmuir* 3 (1987) 198.
- [47] W. van Bronswijk, L.J. Kirwan, P.D. Fawell, *Vib. Spectrosc.* 41 (2006) 176.
- [48] G. Lefevre, *Adv. Colloid Interface Sci.* 107 (2004) 109.
- [49] M. Gräfe, D.L. Sparks, *Geochem. Cosmochim. Acta* 69 (2005) 4573–4595.
- [50] M. Gräfe, M. Nachtegaal, D.L. Sparks, *Environ. Sci. Technol.* 38 (2004) 6561.
- [51] S. Glodberg, C.T. Johnston, *J. Colloid Interface Sci.* 234 (2001) 204.